August 2006

Adaptive Algorithms for 2–Channel Polarization Sensing under Various Polarization Statistics with Non-Uniform Distributions

Konstantin M. Yemelyanov
University of Pennsylvania

Shih-Schön Lin
University of Pennsylvania

Edward N. Pugh Jr.
University of Pennsylvania, pugh@mail.med.upenn.edu

Nader Engheta
University of Pennsylvania, engheta@ee.upenn.edu

Copyright 2006 Optical Society of America, Inc. Postprint version. Published in *Applied Optics*, special issue on "Polarization Imaging and Remote Sensing," Volume 45, Issue 22, August 1, 2006, pages 5504-5520.

Adaptive Algorithms for 2–Channel Polarization Sensing under Various Polarization Statistics with Non-Uniform Distributions

Abstract

The polarization of light carries much useful information about the environment. Biological studies have shown that some animal species use polarization information for navigation and other purposes. It has been previously shown that a bio-inspired Polarization Difference Imaging technique can facilitate detection and feature extraction of targets in scattering media. It has also been established by S. Tyo1 that "Polarization Sum" and "Polarization Difference" are the optimum pair of linear combinations of images taken through two orthogonally oriented linear polarizers of a scene having a uniform distribution of polarization directions. However, in many real environments the scene has a non-uniform distribution of polarization directions. Using principal component analysis of the polarization statistics of the scene, here we develop a method to determine the two optimum information channels with unequal weighting coefficients that can be formed as linear combinations of the images of a scene taken through a pair of linear polarizers not constrained to the horizontal and vertical directions of the scene We determine the optimal orientations of linear polarization filters that enhance separation of a target from the background, where the target is defined as an area with distinct polarization characteristics as compared to the background. Experimental results confirm that in most situations *adaptive* polarization difference imaging outperforms "conventional" polarization difference imaging with fixed channels.

Adaptive Algorithms for 2– Channel Polarization Sensing under Various Polarization Statistics with Non-Uniform Distributions

Konstantin M. Yemelyanov, Shih-Schön Lin
Electrical and Systems Engineering Department, University of Pennsylvania, 200 South 33rd Street, Philadelphia, PA 19104, USA

Edward N. Pugh, Jr.
F. M. Kirby Center for Molecular Ophthalmology and Institute of Neurological Sciences, University of Pennsylvania, 422 Curie Boulevard, Philadelphia, PA 19104, USA

Nader Engheta
Electrical and Systems Engineering Department and Institute of Neurological Sciences, University of Pennsylvania, 200 South 33rd Street, Philadelphia, PA 19104, USA

Abstract: The polarization of light carries much useful information about the environment. Biological studies have shown that some animal species use polarization information for navigation and other purposes. It has been previously shown that a bio-inspired Polarization Difference Imaging technique can facilitate detection and feature extraction of targets in scattering media. It has also been established by S. Tyo[1] that "Polarization Sum" and "Polarization Difference" are the optimum pair of linear combinations of images taken through two orthogonally oriented linear polarizers of a scene having a uniform distribution of polarization directions. However, in many real environments the scene has a non-uniform distribution of polarization directions. Using principal component analysis of the polarization statistics of the scene, here we develop a method to determine the two optimum information channels with unequal weighting coefficients that can be formed as linear combinations of the images of a scene taken through a pair of linear polarizers not constrained to the horizontal and vertical directions of the scene We determine the optimal orientations of linear polarization filters that enhance separation of a target from the background, where the target is defined as an area with distinct polarization characteristics as compared to the background. Experimental results confirm that in most situations *adaptive* polarization difference imaging outperforms "conventional" polarization difference imaging with fixed channels.

OCIS codes: 260.5430 Polarization, 110.2970 Image detection system, 330.1880 Detection, 100.2960 Image analysis, 330.7320 Vision adaptation.

1. Introduction

Polarization is an intrinsic feature of light that provides valuable information about a scene beyond that provided by the scene's spectral (color) and intensity distributions. Polarized light has been studied extensively since Fresnel's investigations of the wave theory, and is important in many areas of modern technology, see e.g.[2, 3, 4, 5]. Polarization information has proven useful in several fields, including computer vision[6, 7], target detection, particularly in imaging targets in scattering media, such as water, fog, etc., in feature extraction[8, 9, 10, 11, 12, 13, 14, 15, 16, 17, 18, 19, 20, 21, 22, 23], and in material classification[25, 24]. Polarization parameters, e.g., Stokes parameters, are in general more sensitive to the nature of a scattering surface than the total intensity is. In such a case, polarization imaging techniques offer the possibility of producing images with higher inherent visual contrast than conventional image processing of the intensity distribution[4].

The polarization of light is not discernible to the unaided human eyes[26], but polarization has been shown to provide valuable information to other species. In 1949, Nobel laureate Karl von Frisch established that honeybees through their perception of polarized light use the sun as a compass through their perception of the polarization pattern of light scattered from the sky[27, 28]. After this von Frisch's discovery other researchers began to investigate polarization vision and found it in many different species, including amphibians, arthropods, desert ants, octopuses, and probably fish (see e.g. Refs.[29, 30, 31, 32, 33, 34, 35, 36, 37, 38, 39, 40, 41, 42]). These animals use polarization information in many different ways, e.g. navigation, detecting water surfaces, enhancing visibility (similar to colors), and perhaps even for mutual communication.

From its utilization by animals, it is clear that the pattern of polarization in an image of a scene is a potentially rich source of information. While the human eye is "polarization-blind", man-made imaging systems have been developed to collect polarization information from scenes[6, 7]. An important issue for such systems is how process and display the polarization information after it is collected by the imaging system to enhance our vision of the scene. Inspired by polarization vision of certain animal species, in earlier studies, our group introduced[13, 43, 44] "Polarization-Difference Imaging" (PDI) processing. We demonstrated that optical imaging systems utilizing PDI techniques may facilitate the detection of targets in scattering media even when the fraction of the light polarized only a few percent, and that such enhancement can increase by up to 3-fold the distance over which targets can be reliably detected near threshold visibility[43, 13, 44]. We have also investigated the issue of optimal representation of polarization information for the "polar-blind" human eye[44, 45, 46].

The idea that polarization vision may involve adaptation to the environmental polarization is bio-inspired as well. Insects employ a retinal filter consisting of an array of ommatidia (polarization sensitive photoreceptors) that is approximately "matched" to the polarization pattern of the sky[33]. This filter works as follows: The summed output from all polarization analyzers of the polarization sensitive area reaches a maximum when a "match" between the receptor array and the celestial pattern has been approximately achieved. This provides the insect with the information of how to align its longitudinal body axis with the symmetry plane of the sky. In order to find a proper direction, the insect has to change its orientation and perform a "check" of polarization pattern for each angle of orientation.

Inspired by a concept of "matched filter"[32, 33], we develop here a polarization imaging technique based on PDI, but "adaptable" to the environmental conditions, i.e., to the polarization "background" of a scene. The proposed polarization-based system adaptively adjusts itself to enhance the segregation of targets from the background in a manner dependent on the

polarization statistics of the scene.

The paper is organized as follows: in Section 2, we give a brief overview of polarization concept and define the polarization parameters used in the paper. In Section 3, we describe the Adaptive Polarization-Difference Imaging (APDI) algorithm. Section 4 is devoted to validation of the proposed technique, employing both experiments and simulations. In Section 4, we illustrate the performance of the algorithm in target-against-background detection using the experimental data obtained in a natural environment. In Section 5, we apply the APDI algorithm to a scene taken under natural illumination condition. In Section 6 we propose an APDI-based method that may be used in surveillance systems, compare APDI with several other methods in polarization-based imaging, and discuss performance of the algorithm. And finally in Section 7, we present the conclusions.

2. Physics of polarization imaging

The polarization of a local field of monochromatic coherent light source can be represented as a superposition of two mutually orthogonal wave components. A phase difference between these components produces a linearly, elliptically, or circularly polarized wave with its polarization direction determined by the relative strengths of the components. Since human eyes and most conventional camera sensors can only detect the total light intensity collected at each pixel during an exposure time many time longer than the oscillation frequency, when the light energy is uniformly distributed over all polarization directions, the detected signal will be the same for any polarization direction. Such light is called "unpolarized" and emitted by most common light sources, including the sun or man-made incandescent light sources. The local polarization signal at the surface of a sensor (that cannot detect phase information) can be described as a combination of unpolarized and completely linearly polarized components.

Assuming that a perfect linear polarizer is placed in front of a normal polarization-insensitive device, such as a CCD or film camera, the observed intensity $I(x,y,\varphi)$ at the pixel located at (x,y) is in general a function of the angle φ that polarization analyzer makes with a reference direction, and can be described as:

$$I(x,y,\varphi) = I_U(x,y)\left\{1 + p(x,y)\cos\left[2\left(\theta(x,y) - \varphi\right)\right]\right\}, \tag{1}$$

where I_U is a half of the total pixel intensity, and p is the degree of *linear* polarization, defined as $\left[I_{\max}(x,y) - I_{\min}(x,y)\right] / \left[I_{\max}(x,y) + I_{\min}(x,y)\right]$ where $I_{\max}(x,y)$ and $I_{\min}(x,y)$ denote at each pixel (x,y), respectively, the maximum and minimum observed intensity within a full rotation of the analyzer. (We note that this definition of degree of *linear* polarization, which is more suitable for wideband signals used here, is different from what is used as the degree of polarization in the context of the Stokes parameters[52]). Everywhere in this paper, we use the horizon as the reference direction and angles increase counter-clockwise relative to the direction of the horizon.

As evident from Eq. (1), at each pixel of the image of a scene the polarization (and intensity) of the impinging light is characterized by three independent parameters: thus, in order to obtain complete information about the polarization features of the object, at least three measurements of light intensity at different angles φ are required. These measurements can be made either simultaneously by three CCD cameras, such that each camera has a fixed polarizer

set at a different angle, or (assuming the scene stable over time) by one camera taking imaging sequentially through a polarizer oriented at three different angles. Our computational algorithm can be used with either measurement method after proper calibration.

Consider three images of a scene, I_0, I_{45}, I_{90}, corresponding to three angles of orientation of the linear polarizer, namely, $\varphi = 0^\circ$, 45° and 90° with respect to the reference direction. From these three images, we can calculate I_U, p, and θ at each image point as follows:

$$
\begin{aligned}
I_U(x,y) &= \left[I_0(x,y) + I_{90}(x,y) \right] / 2 \\
p(x,y) &= \left[\left(1 - \frac{I_{45}(x,y)}{I_U(x,y)} \right)^2 + \left(1 - \frac{I_{90}(x,y)}{I_U(x,y)} \right)^2 \right]^{1/2} \\
\theta(x,y) &= \frac{1}{2} \tan^{-1} \left[\frac{I_U(x,y) - I_0(x,y)}{I_U(x,y) - I_{45}(x,y)} \right]
\end{aligned}
\tag{2}
$$

Once the parameters I_U, p, and θ are computed for each pixel of the scene image, one can reconstruct the image intensity that would be observed for any angle φ using Eq. (1), even though no actual pictures are taken with a polarizer oriented at φ.

3. The concept of Adaptive Polarization-Difference Imaging

A. Polarization Difference Imaging (PDI)

The concept of PDI was introduced in earlier investigations of our research group[13, 43, 44, 45, 46]. This idea has since been utilized by other research groups (see e.g. Refs.[14, 19, 21, 49, 50, 51]). The original PDI system captures images of a scene at two orthogonal linear polarizations. Thus one obtains a pair of images, i.e., $I_0(x,y)$ and $I_{90}(x,y)$ taken at 0° and 90° orientation of the polarizer, respectively. The "Polarization Sum" (*PS*) and "Polarization Difference" (*PD*) images are linear combination of the intensity images for the two orthogonal polarizations: thus, given $I_0(x,y)$ and $I_{90}(x,y)$ one computes:

$$
\begin{bmatrix} PS(x,y) \\ PD(x,y) \end{bmatrix} = \underbrace{\begin{bmatrix} 1 & 1 \\ 1 & -1 \end{bmatrix}}_{T} \begin{bmatrix} I_{90}(x,y) \\ I_0(x,y) \end{bmatrix},
\tag{3}
$$

where T identifies the transformation matrix. For an ideal linear polarizer the *PS* image is equivalent to a conventional intensity image.

Tyo has shown[1] that the two image channels *PS* and *PD* given by Eq. (3) are the principal components (PCs) of a scene in which the polarization angle has a uniform distribution: thus, in such a case, *PS* and *PD* are optimal channels in the information-theoretic sense of carrying maximally uncorrelated information about the scene. Tyo's ideas were developed in analogy with a principal component analysis (PCA) of trichromatic (3-cone pigment) color vision by

Buchsbaum and Gottschalk[54]. In Tyo's analysis, as in that by Buchsbaum and Gottschalk, the transformation matrix T in Eq. (3) is derived by applying PCA to the covariance matrix of the input channels (e.g., I_0 and I_{90} in Eq. (3)) for a "broadband" distribution of the relevant property (polarization, spectral distributions) over the ensemble of scenes. In these analyses the principal component with the largest eigenvalue is a same-signed sum of the input channels, while the remaining components are "opponent", involving opposite-signed weighting coefficients in the transmission matrix[1, 54]. An interesting corollary to the optimality of PCA channels in information encoding is that the opponent channels can also be understood to be optimized for the detection of change relative to the average scene to which the first principal component is "tuned": thus, the opponent channel(s) in effect perform a common-mode rejection of the statistically average scene or "background" signal, and in doing so enhance the signal-to-noise ratio (*SNR*) and thus the detectability by the opponent channels of targets in a scene that differ in polarization statistics from the background. This duality in the sense of optimality of PCA-derived channels led us to seek the optimum channels for an arbitrary background scene.

B. Generalization of PDI to non-uniform polarization statistics

In real scenes, both the polarization orientation and the degree of linear polarization of the scene have non-uniform distributions. In such situations the *PD* signal of Eq. (6) may not be the most useful signal for detecting targets against the average background. What would then be the appropriate image (i.e., a combination of signals) to reveal hidden polarization features of the scene and improve the target detection? Answering this question is the goal of this study.

Our approach to this goal has been to enable our imaging system to "adapt" to the polarization statistics of the background, so that if any changes occur in the scene they will "pop out" on one of the channels. The adaptation of the system to the polarization statistics of the background in effect performs a common mode rejection of the background. In such an approach, it is assumed here that the system measures the polarization statistics of the scene in the two different stages: once when only the background is present, and again when a target is present with the background. Furthermore, in describing the ideal behavior of such a system, the target is considered as a perturbation of the background scene, i.e. a minor change that does not alter the overall polarization statistics (Section 4C).

Consider the general case such that the probability density function of the polarization angle over the pixels is arbitrary. Assume that images of the scene with $M \times N$ pixels have been taken with two different orientations (not necessarily orthogonal) of the polarizer, i.e., $I_1 = I(\varphi_1)$, and $I_1 = I(\varphi_2)$. Here we examine these two signals using the PCA technique[56]. According to PCA, the covariance matrix for such an arbitrary pair of images is defined as:

$$C(\varphi_1, \varphi_2) = \begin{bmatrix} E[I_1 I_1] - E^2[I_1] & E[I_1 I_2] - E[I_1]E[I_2] \\ E[I_1 I_2] - E[I_1]E[I_2] & E[I_2 I_2] - E^2[I_2] \end{bmatrix}, \tag{4}$$

where $E[W] = \frac{1}{MN}\sum_{m=1}^{M}\sum_{n=1}^{N} W(x_m, y_n)$ is the mean value taken over the ensemble of pixels in the images, and W is equal to I_1, I_2, or a product thereof. Once the eigenvalues (λ_1, λ_2) and the eigenvectors of the covariance matrix C are determined, the transformation matrix, which has the eigenvectors as its rows, is formed as follows:

$$T(\varphi_1,\varphi_2)=\begin{bmatrix} -\beta(\varphi_1,\varphi_2) & \alpha(\varphi_1,\varphi_2) \\ \alpha(\varphi_1,\varphi_2) & \beta(\varphi_1,\varphi_2) \end{bmatrix}. \tag{5}$$

The signs of the scalars α and β may be either positive or negative. The transformation matrix is formed in such a way that the first eigenvector corresponds to the largest eigenvalue. The "principal component" images are then computed as follows:

$$\begin{bmatrix} PC_1(\varphi_1,\varphi_2) \\ PC_2(\varphi_1,\varphi_2) \end{bmatrix} = T(\varphi_1,\varphi_2)\begin{bmatrix} I(\varphi_1) \\ I(\varphi_2) \end{bmatrix}. \tag{6}$$

By analogy with the transformation matrix of Tyo's "conventional" PDI system, we consider PC_1 the "adaptive" analog of the *PS* signal, and the PC_2 the analog of the *PD* or "opponent" signal. Our surmise was that by analyzing the PC_2 image of a scene, certain important features, e.g. the detection of target in presence of a standard background will be enhanced.

All the parameters in Eqs (5) and. (6) are functions of the two polarizer angles, which in general need not be orthogonal. For the case of a uniform distribution of polarization ellipse orientations over the scene, Eq. (6) reduces to Eq. (3). Our goal is to identify a pair of analyzer angles and a pair of weighting coefficients in Eq. (6) (i.e., the components of the eigenvectors shown in Eq. (5)) that yield a PC_2 image that "optimally" enhances the visualization of novel targets in a specific background scene. The term "optimum" here is used by analogy with the approach previously used in analyses of color vision and polarization vision, as described in Section 3A. In those analyses a formal assumption was made about the properties of the ensemble distribution of signals. In the present analysis, the role of the ensemble distribution is played by the polarization distribution of a specific background scene, and so we will put the adjective "optimum" in quotations, with the understanding that it is our task to demonstrate empirically that the method indeed yields a practical optimum separation of targets from the specific background.

C. Finding a transformation matrix to adapt the PDI system to a specific background

To adapt the PDI system to a specific background scene, we first obtain complete polarization information on the background: specifically, we capture three images of the background scene for three orientations of the polarizer and then compute the polarization parameters that completely characterize the scene with Eq. (2). From these results, we can synthesize images of the scene corresponding to any angle of orientation φ of the polarizer with Eq. (1). It bears emphasis that derivation of images corresponding to various polarizer orientations φ from the initial set of three images is not linear.

The next step is to perform principal components analysis as described in Subsection 3B for a wide selection of pairs of angles φ_1, φ_2, deriving the transformation matrix $T_{BG}(\varphi_1,\varphi_2)$ of Eq. (6) for the background for all pairs of angles. This yields a table or map of the derived polarization parameters over the 2-dim space of angles: i.e., $\alpha(\varphi_1,\varphi_2)$, $\beta(\varphi_1,\varphi_2)$, $\lambda_1(\varphi_1,\varphi_2)$, and $\lambda_2(\varphi_1,\varphi_2)$ for $0 \le \varphi_1,\varphi_2 \le 180^\circ$. It is reasonable to expect that the "optimum" pair of angles will be that with corresponding extreme eigenvalues. When the "optimum" pair of angles is

chosen, then Eq. (9) is applied to the "target" scene. Here we consider in particular the following possible choices for the "optimum" pair (φ_1, φ_2) of polarizer orientations:

Case 1. the pair that maximizes the eigenvector component α (and it minimizes the magnitude of β);
Case 2. the pair that maximizes/minimizes the eigenvalues;
Case 3. the pair of orthogonal angles that has the preferential angle of the background polarization as its bisector.

Consideration of Case #3 will allow a comparison between the conventional PD algorithm and the new adaptive algorithm here. In this case, as the preferential angle of polarization we understand the angle corresponding to the modal value of the empirical distribution of polarization angles over the pixels corresponding to the background scene. We initially focus our investigation on Cases #1 and #2, and then compare the results with those obtained for Case #3. Practically, the APDI system images the scene at two consecutive stages. The information obtained at the first stage is assigned to the "background" scene (where no target is present), and the information obtained at the second stage is assigned to the "target" scene (where the target and the background are present).

4. Validations of the APDI Algorithm and the Selection of the "Optimal" Set of Parameters

To develop the APDI approach and examine its utility, we conducted several sets of experiments and simulations. The first set of images was taken in our laboratory – a controlled environment with stable illumination conditions. The target was a specially designed object with known polarization properties, and the background, as we will describe, was kept simple, while still exhibiting non-uniform polarization statistics. This enabled an accurate evaluation of the performance of APDI for the target detection. The second set of images was taken with real-life targets under natural illumination (sunlight).

A. Experimental setup in the laboratory

The laboratory experimental setup and a specially manufactured target are shown in Figure 1. Incandescent 150 W lamp was illuminating the cylindrical Plexiglas tank (12" height and 16" in diameter) from a side. The tank was filled with a solution of a 10 mL of whole milk diluted in approximately 27 L of water. The height of the water level in the tank was 21 cm. This created a model of dispersive media (such a method of simulation of scattering media was originally used by Tyo et al.[13]). In order to produce Lambertian type illumination, an opal glass diffuser was placed between the tank and the light source. The target was an aluminum disk with 5.1 cm in diameter. The target surface was sandblasted and there were seven 1-cm^2 square patches on it (see Figure 1b). The six outer patches were abraded with emory paper in such a way that they formed three orthogonally oriented pairs, i.e., 0° and 90°, 30° and 120°, 60° and 150° (with respect to the vertical axis). Patches with orthogonal directions in the scratches are located diametrically opposite each other. The surface of the center patch was sandblasted the same way as the base plate surface. The patches were raised a few mils from the base plate surface. The target was attached to the Plexiglas plate and facing up. The distance between the surface of the water ant the plane of the aluminum disk was 55 mm. The target was observed by an Olympus E-10 SLR digital camera with Sunpack® 62 mm diameter glass polarizer attached in front of it. The images were taken sequentially for three different orientations of the polarizer, i.e., 0°, 45°,

and 90° degrees by manually rotating the polarizer between shots. All the images in the laboratory experiment were taken with exposure time of 1 second and F-number of the camera equal to 4.0. During such exposure time any fluctuations due to 120 Hz oscillations in the light source are therefore averaged out. The total time required to capture all three images was less than 10 seconds and was limited mainly by the time required to save the raw image of the scene to the camera's flash memory. The same digital camera and polarizer were used in our experiments in the natural (uncontrolled) environment.

All computer analyses in this study have been done using "MATLAB®" software package with its "Image Processing Toolbox". The captured images were stored in Olympus Raw Format (ORF), which gave us "raw" images of the scene, without the enhancements and modifications that most commercial digital cameras perform internally to make pictures "look better". The Olympus E-10 has a single chip color CCD with RGGB Bayer primary color filter. For our computations, we extracted the R, G, and B components of the RGB (red-green-blue) output directly from the RGGB Bayer filter pattern response, so that the image had only ¼ the total number of active pixels of the CCD chip (the G image is an average value of the two G filter responses). PCA may be applied to any pair of polarization channels capturing images representing one of the components (either R, G, B or V). The V (luminance) component of the HSV (hue-saturation-luminance) was computed by the MATLAB® Image Processing Toolbox and was, in fact, the maximum value of the R, G, or B channel at every pixel. In this paper we present results which were obtained based on the V component of the images.

The camera zoom was adjusted in such a way that the area occupied by the aluminum disk was only a portion of the target scene. In order to obtain the "background" scene, we simply removed the aluminum disk from the scene while keeping all other experimental conditions, including the focusing distance of the camera, intact. The original image was cropped to 800 by 600 pixels for efficiency in analysis. The polarization statistics of the background scene are shown in Figure 2. The histograms of the polarization parameters reveal a non-uniform distribution of the polarization statistics of the scene with the average degree of linear polarization of about 25%.

Throughout this paper we present grayscale images with double precision, i.e., ranging from 0 to 1, where 0 corresponds to 0 and 1 corresponds to 255 of 8-bit gray scale. In order to assess the intrinsic noise of the camera, we made measurements with the camera lens covered by an opaque cap. The histograms of the standard background's half intensity distribution, i.e., I_U are compared with the histogram of the "dark noise" image in Figure 3. The mean value of the camera-noise image is 0.5×10^{-2} and standard deviation is 7×10^{-4}, while for the background intensity image those parameters were 0.95×10^{-1} and 0.22×10^{-1}, respectively. Thus, intrinsic camera noise is negligible in the standard conditions of the experiments.

B. Application of APDI algorithm to images obtained in controlled environment

Eq. (1) was applied to images of the background taken at three orientations ($\varphi = 0^\circ$, 45° and 90°) of the linear polarizer, and then images were generated for each angular orientation of the polarizer within the range from 0 to 180 degrees with 5 degrees step (φ and $\varphi+180^\circ$ are indistinguishable cases since phase information is not encoded by the camera). For each pair of images of the background corresponding to the pair of analyzer orientations (φ_1, φ_2) we then

extracted a full set of polarization parameters using PCA, i.e., $\alpha = \alpha(\varphi_1, \varphi_2)$, $\beta = \beta(\varphi_1, \varphi_2)$, $\lambda_1 = \lambda_1(\varphi_1, \varphi_2)$, and $\lambda_2 = \lambda_2(\varphi_1, \varphi_2)$ (Figure 4).

The distributions of $\alpha(\varphi_1, \varphi_2)$ and $\beta(\varphi_1, \varphi_2)$ have similar forms, and in particular have their maxima and minima at the similar locations in the space (φ_1, φ_2). The eigenvalues λ_1 and λ_2 are symmetric functions of (φ_1, φ_2), i.e., $\lambda_i(\varphi_1, \varphi_2) = \lambda_i(\varphi_2, \varphi_1)$ for i = 1, 2. The maximum and the minimum values of λ_1 are located on the line of symmetry $(\varphi_2 = \varphi_1)$, which represents the situation when the angle of the linear polarizer for both source images is the same, and is obviously not useful. Therefore, Case #2 reduces to the analysis of behavior of the smaller eigenvalue, i.e. λ_2. The value of λ_2 represents the variance in the PC_2 image, suggesting that more interesting information can be obtained from the PC_2 image.

The APDI algorithm was applied to each "target-background" pair, and PC_1 and PC_2 images for all three cases described in Subsection 3C above were computed, and the corresponding parameters are given in Table 1. PC_1 and PC_2 images for all three cases are illustrated in Figure 5. The PC_1 images for the three cases are very similar, and in particular the non-uniform illumination of the scene is clearly visible in each. The PC_2 images in panels *b*) and *c*) of Figure 5 are similar because the pairs of angles derived for Cases #2 and #3 are close to each other, as well as the corresponding polarization parameters (see Table 1). However, the PC_2 image corresponding to Case #1 (Figure 5*a*) is noticeably different: the margins of the disk are more clearly outlined, and the direction of scratches in all the patches (which vary in polarization orientation), are distinguishable. The clear segregation of the disk from the background in the PC_2 image is achieved in large part due to the lower variance of the background scene in this channel, as we now describe.

In Figure 6 we present normalized (i.e., unit area) histograms of the PC images for all cases considered. The distributions and in particular the standard deviations of the PC_1 images are very close for all three cases ($\sigma_i^2 \approx 0.5 \times 10^{-2}$). In contrast, for the PC_2 images the standard deviation for Case #1 ($\sigma_1^2 = 3.68 \times 10^{-3}$) is more than 50% lower than in the other two cases (Case #2, $\sigma_2^2 = 8.62 \times 10^{-3}$; Case #3, $\sigma_3^2 = 8.53 \times 10^{-3}$). Thus, the PC_2 image for Case #1 has the smallest variance in the distribution of pixel intensities, suggesting that Case #1 may provide an "optimum" set of adaptive parameters for the detection of novel targets in PC_2 images.

C. Performance evaluation of APDI: Sensitivity index

The selection of the "optimum" transformation matrix for a specific background should both lead to a minimum variance in the PC_2 image of the background, and enable targets with novel polarization properties to "pop out" in the PC_2 channel. To avoid relying only on evaluation of the images of targets by human viewing, we employed an objective numerical evaluation: the sensitivity index calculation. The sensitivity index is based on the Signal-Detection Theory (SDT), which quantifies an observer's ability to discriminate a target from a background[55]. In SDT, an observation taken at some moment may arise from a "noise alone" distribution, or from the "signal-plus-noise distribution," with the means of these distributions separated by a certain amount d_a specified in units of the standard deviations; d_a is called the sensitivity index. With increase of d_a, the probability of successful target detection (a "hit") will increase, since the overlap between the distributions decreases, and the probability of a false alarm will also

decrease. In our study as the "signal-plus-noise distribution" we consider the scene distribution including both the target and background, while the "noise-alone distribution" is taken as the scene distribution without the target present.

To estimate d_a empirically, we performed a series of measurements with 3 minutes separation between each set. The experimental setup was as described in the previous subsection. We first captured 20 sets of images of the background alone, and then 20 sets of images of the background-plus-target scenes; each set of images comprised 3 images collected at $\varphi = 0^\circ$, 45° and 90°, allowing derivation of an equivalent image for any polarizer orientation φ and PCA, yielding PC_1 and PC_2 images for Cases #1-3. An "observation" for the SDT analysis was computed over two square regions of 5 by 5 pixels, determined by the imaged location of special portions of the target (Figure 7). For each of the 20 sets of images of the background and the background-plus-target scenes, the average intensities of these regions in the PC_1 and PC_2 images were calculated. In summary, we ended up with 20 pairs of observations of the PC_1 and PC_2 values for these two specific regions of the scene for each of the three cases. We then estimated the sensitivity index as

$$d_a = \left| \frac{\mu_T - \mu_B}{\sqrt{\left(\sigma_T^2 + \sigma_B^2\right)/2}} \right|, \tag{7}$$

where μ_B and σ_B^2 are the mean and the variance of the background scene in the specific region, and μ_T and σ_T^2 are the mean and the variance of the same region when the target object is present[55]. The values of the sensitivity index for PC_2 images corresponding to the three cases (and the two target regions respectively) were as follows: Case #1, $d_a = 1.703$, and $d_a = 1.687$; Case #2, $d_a = 0.772$ and $d_a = 1.371$; Case #3 $d_a = 1.419$ and $d_a = 0.908$, respectively. Here the first value of d_a in each case corresponds to the left-hand side target region and the second value to the right-hand side region, respectively (Figure 7). The parameters determined by Case #1 clearly yield superior detectability of the polarization targets than those determined by Cases #2 and 3. Remarkably, the Case #1 PC_2 channel outperforms the PC_2 channel of the other two cases on *both* the left and the right targets, even though each of these other channels performs much better on one of the two targets. These observations suggest that the PC_2 channel generated with the maximum components of eigenvectors (α, β) correspond to the "optimum" pair of angles for detection of polarization targets against a polarized background.

5. Target Detection against a Non-Uniformly Polarized Background under Natural Illumination Conditions

In addition to the experiments in the lab, we performed several experiments under natural illumination conditions. As in the laboratory, every experiment session include capturing three images of both the background scene and the target scene. Unlike the lab experiments, where the background was a largely a uniform scene, in this situation the background is a relatively complex one, and contains several different objects.

The first experiment presented here was done inside the Levine Hall of the University of Pennsylvania. The images for this experiment show the stone floor surface of the hall (Figure 8).

The scene consisted of the shadow region formed on the floor by the combined shadows of an upright standing person and the window frame. The rest of the scene was illuminated by the sunlight passing through the window glass. The camera was located opposite to the window and elevated above the floor, thus the scene was illuminated by sunlight in such a way that the light beam coming from the sun and a beam reflected from the scene formed the same plane. The floor was of mainly dark grey color with a broad pattern. The "target" object was a translucent plastic case of a CD. We took three images of the background and of the target scenes. The camera settings were kept the same for both the background-only image sets and the image sets with the target in the scene. The exposure time for each image was 1/8 second and F-number of the camera was equal to 8. Figure 8 shows three polarization components (I_U, p, and θ) for both the background and the target scenes, placed side-by-side for easy comparison: the target object has a lower degree of polarization than surrounding background.

Using the ADPI Case #1 algorithm, the "optimum" pair of angles are found to be $\varphi_1 = 140^\circ$ and $\varphi_2 = 50^\circ$, with eigenvector components $\alpha = 0.9965$ and $\beta = -0.0834$. The histogram of the background angle of polarization shows that the preferential angle of polarization of the background is approximately $\theta_B = 140^\circ$, which means that the optimal angle pair is the angle of preferential polarization and the angle orthogonal to it. The angles corresponding to the maximum and the minimum of the larger eigenvalue (i.e., λ_1) are found in the bisector line of eigenvalue surface, where $\lambda_1^{\max}$ is located at the point $\varphi_1 = \varphi_2 = \theta_B$, and $\lambda_1^{\min}$ is located at the point $\varphi_1 = \varphi_2 = \theta_B \pm 90^\circ$. This information can be useful: if the preferential polarization angle is known *a priori* then the "optimal" angle pairs can be found directly without time-consuming computation. On the other hand this can be an effective way to recover the preferred polarization direction in a scene.

Comparing the principal component images of the scene (panels *b*) and *d*) in Figure 9) one may see a significant improvement in the target/background contrast of the PC_2 image over the conventional *PD* image. In order to have a more comprehensive comparison, we included also images that correspond to the pair of angles bringing the smaller eigenvalue to the maximum (Case #2), i.e., consider images with the minimum variance in intensity. For this experiment, the maximum value of λ_2 is found at $\varphi_1 = 105^\circ$, $\varphi_2 = 15^\circ$ and the corresponding coefficients are $\alpha = 0.5016$, $\beta = -0.8650$. Principal component images created in this case are also presented in Figure 9 (panels *g*) and *h*)). Although an improvement over the conventional *PD* image (Case #3) is noticeable (comparing panels *d*) and *h*) in Figure 9), the pair of angles determined by Case #1 yields better results. Overall, then, we conclude that Case #1 yields the "optimum" PC_2 channel.

6. Discussion

We have presented the mathematical basis of a novel "adaptive" PDI technique, and experimental results which demonstrate its performance in target detection applications. For scenes with uniform distributions of polarization parameters, APDI reduces to conventional PDI technique. However, in many real world situations, APDI will yield superior performance, so that targets with polarization features can be more readily detected against a background.

A. Summary of the APDI algorithm

For the discussion to follow, it is useful to summarize the APDI algorithm:

1. Capture three images of the "background" scene for three different orientations φ of the linear polarization analyzer.
2. Process those three images and obtain complete polarization statistics of the "background" scene according to Eq. (2).
3. Synthesize polarization images of the scene for the full range of angles of orientation φ of the polarization analyzer using Eq. (1).
4. Perform Principal Components Analysis on all possible pairs of angles and obtain four adaptive parameters as functions of angle of polarizer's orientation, the two eigenvector components, and the two eigenvalues.
5. Find the "optimum" set of adaptive parameters (Case #1) and create the transformation matrix of the background scene, i.e., $T_{BG}\left(\varphi_1^{opt},\varphi_2^{opt}\right)$.
6. Repeat steps 1 and 2 for the scene with the target present.
7. Synthesize a pair of polarization images of the "target" scene for optimal pair of angles $\left(\varphi_1^{opt},\varphi_2^{opt}\right)$ as found in step 5.
8. Using the transformation matrix that was obtained from the background scene, $T_{BG}\left(\varphi_1^{opt},\varphi_2^{opt}\right)$, create principal component images of the "target" scene according to Eq. (6).

Since the APDI algorithm deals with the polarization statistics of the scene, if the target occupies only a small portion of the scene, adaptive coefficients and "optimal" pair of angles obtained from statistics of the "background scene" will differ little from those obtained from the statistics of the "target scene". Thus the APDI algorithm may be applied to the target scene directly without gathering additional information from the background. However, if the target object occupies a significant portion of the image, a complete set of measurements of the background is required in order to segregate the target object from the background. Although in this study we dealt with scenes that had a non-uniform distribution in polarization parameters, the polarization of the background had only one preferential direction of polarization. If the scene has two or more regions of significant areas that have different angles of preferential polarization, further improvements may be required, such as segmentation of the scene based on its polarization statistics. Such results will be reported in our subsequent paper.

The APDI algorithm is relatively fast and does not require significant computer resources. For the computer workstation with Pentium® 4 550 processor and 2 GB of RAM, the total computational time was about 30 seconds using the code written in MATLAB. Rewriting the code using less resource aggressive programming language, such as C++ will significantly reduce the processing time. The time required for capturing the images may be also reduced. Currently in the laboratory we employ a setup where the rotation of the polarizer is performed by a stepping motor and the entire process can be controlled from the computer. Use of this setup will automate the procedure of capturing images and their transition to computer.

B. Potential applications

Based on the computer simulations and experiments presented above we propose the APDI algorithm for use in detection of targets with polarization features. To speed the process, the initial pair of angles may be selected such that one of the angles is equal to the preferential polarization angle of the background and the other angle chosen to be orthogonal to the

preferential angle. In order to ensure that the selected pair is "optimum", the calculations of adaptive coefficients for a few pairs of polarizer orientations around the selected point should be performed. The pair with the maximum component value of the eigenvectors is then used as the optimal pair. This approach may significantly decrease the computational time, as is very important for real-time applications.

C. The sensitivity of the APDI algorithm to the rotation of the pair of angles

Since the APDI algorithm may be used as an effective tool in a visual surveillance system, an important issue in this application is: "how sensitive are the adaptive pairs to rotation of the polarization channels?"

Assume that by applying the APDI algorithm an "optimum" set of (Case #1) parameters has been found. Consider then rotating this pair by certain angle clockwise or counter-clockwise. Would it be possible to obtain a PC_2 image of the same quality? A simulation of the sensitivity of the APDI algorithm to such rotations was undertaken with the same set of experimental data reported above. The adaptive coefficients were applied to the pair of images corresponding to angles rotated by 5 and 10 degrees from the "optimum" (Case #1) pair. The goal was to check in which case the aluminum disk is better detectable against the surrounding water solution. For each case we calculated the Signal-to-Noise Ratio (*SNR*), considering the output from the aluminum disk as the signal and the output from the surrounding water solution as the "noise" or background. Thus, we derived

$$SNR = \left| \frac{\mu_D - \mu_W}{\sigma_W} \right|, \tag{8}$$

where μ_D is the mean value of pixels belonging to the aluminum disk, μ_W, σ_W are the mean value and the standard deviation of all the image except the aluminum disk, respectively. Figure 10a shows *SNR* for PC_1 and PC_2 corresponding to optimal pair angles and for pairs of angles rotated by 5 and 10 degrees with respect to optimal pair. One may notice that the *SNR* for the optimal pair of angles is the highest and rapidly decreases with rotating of the polarizers. With rotation of the angle pair, both the background level and its variance increase, while the intensity level of the target remains at approximately the same level. This can be seen in the histograms of the PC_2 images for the area surrounding the aluminum disk (see Figure 10b).

These results show that a shift in the pair of angles from those determined by Case #1 may decrease the *SNR* for a target object against the surrounding background.

D. Effects of noise on the performance of APDI

In this subsection we discuss the influence of noise on the performance of our technique. In order to evaluate the performance of APDI, we artificially added noise to a set of input images, I_0, I_{45}, and I_{90} for both "background" and "target" scenes. We used two types of noises, i.e., white noise and Gaussian noise with a mean values in both cases equal to the mean values of input images. The standard deviation for the Gaussian noise was selected as a certain percentage of the dynamic range of the input images, i.e., the mean value of input images was multiplied by a coefficient which varied from 0.01 to 0.21. For the white noise, the range of variations was the same as the standard deviation in the case of Gaussian noise. Once the noise was added to input images, the polarization components were recovered and then the APDI procedure as described

in Subsection 6A was done. For each percentage of noise we calculated *SNR* according to Eq. (8) for both PCs corresponding to optimal pair of angles, for conventional *PS* and *PD* images, and for the degree of linear polarization p. The results are shown in Figure 11. One may notice that APDI is more sensitive to the presence of Gaussian noise than to the white noise. After certain amount of noise the *SNR* calculated using the image of p becomes slightly higher than those for the PC_2, although individual features of the target, such as patches are not detected in the image of p, it is detected in PC_2 (compare panels C) and D) in Figure 11, where that images are shown with addition of 5% of noise). With increasing amount of noise, the performance of the APDI algorithm decreases, but still for the case of white noise even with the amount of noise about 20%, the performance of APDI is higher than those of conventional PDI.

E. APDI compared to other polarization analysis techniques

In order to produce the polarization-difference images, either a scene is illuminated by natural light and the scattered light is analyzed with the two orthogonal polarizers or a scene is illuminated with the two light sources of orthogonal polarizations. The idea of weighed subtraction of the two orthogonal component of the scene was first introduced by Walker et al.[19]. Their method involves subtraction of a scaled image obtained at one polarization from the oppositely-polarized image, and shows improvement over methods in which subtraction is done without scaling. In this study the image contrast was evaluated as a function of the scaling of the subtracted image, and the orthogonal polarization axes were fixed. In contrast, the APDI algorithm presented here adaptively selects two orientations of the polarizer, and also finds the "optimum" weighting of the resultant images by employing PCA to derive the transformation matrix (Eq. (5), (6)), and thereby the resultant PC_1 and PC_2 images.

Several publications have discussed nonlinear aspects of polarization imaging techniques, see e.g.,[11, 12, 14]. The APDI algorithm proposed here is essentially linear once PCA analysis has been applied to the background (derivation of the images of the background corresponding to a full set of orientations of the polarizer involves the nonlinear equations, Eq. (1) and (2)). An advantage of the APDI method includes the fact that it is readily applicable to many different kinds of scenes in which polarization affects image intensities, including scenes that include specular reflection (e.g. Figure 9), underwater scene (Figure 5), and low light scenes in which either natural or artificial illumination is used. Moreover, APDI can be implemented without using specialized equipment: only a digital camera and polarizer are required for capturing images.

It has been proposed that images of the degree of linear polarization in a scene[7, 8, 20] (cf. $p(x,y)$ in Eq. (2)) may provide a valuable tool for detection and discrimination of objects. Such images no doubt have considerable value, and can be readily implemented with the tools employed here. While we have not performed an exhaustive comparison, we can confidently assert that the signal obtained with PC_2 of APDI outperforms that obtained from p images in the cases we have examined; one such comparison is provided in Figure 12. In this case the variance of the background in the PC_2 image is about $1/10^{th}$ that of the p image. As a result, the *SNR* calculated according to Eq. (8) is higher for the PC_2 vs. the p image: 3.056 vs. 2.417. Nonetheless for the superior *SNR* of APDI, under conditions where speed is critical, use of the p image for rapid initial inspection should be quite valuable, and it bears emphasis that the p image data are automatically generated in the APDI algorithm.

7. Conclusions

We have developed a set of techniques to form an "optimum" linear combination for the polarization channels that is adapted to the polarization statistics of a scene. Utilizing the technique of Principal Components Analysis, we have determined an optimum linear combination of polarization channels (Eqs. (5), (6)) to produce PC_2 images that efficiently provide information for discriminating a target with polarization properties from the background scene. The adaptive transformation is readily adjusted as the imaging system observes different environments or varying lighting conditions. The adaptive transformation is particularly suitable for environments with preferential polarization distribution. This approach may point to an interesting research direction in the polarization vision in certain aquatic species, which may have detector arrays that act like adaptive PC_2 channel. A further utility of the APDI system is that once the polarization information (see Eq. (2)) fully characterizing the background scene has been collected (e.g. by a surveillance system that routinely takes images at three orientations of a linear polarizer), the image data may be processed off-line to yield optimum presentation of polarization features of the scene that may otherwise escape attention.

8. Acknowledgements

This work was supported by the U.S. Air Force Office of Scientific Research (AFOSR), through grants F49620-01-1-0470, F49620-02-1-0140, FA9550-05-1-0052, and the DURIP grant F49620-02-1-0241. We would like to thank the anonymous reviewers for their useful comments.

9. References and notes

1. J. S. Tyo, "Optimum linear combination strategy for an N-channel polarization-sensitive imaging or vision system," J. Opt. Soc. Am. A **15**, 359–366 (1998).

2. W. A. Shurcliff, *Polarized Light, Production and Use* (Harvard University Press, Cambridge, 1962).

3. D. Goldstein, *Polarized Light* (Marcel Dekker, Inc., 2003).

4. J. E. Solomon, "Polarization imaging," Applied Optics **20**, 1537–1544 (1981).

5. S. Demos and R. Alfano, "Optical polarization imaging," Appl. Opt. 36, 150-155 (1997).

6. L. B. Wolff, "Polarization camera for computer vision with a beam splitter," J. Opt. Soc. Am. A **11**, 2935–2945 (1994).

7. L. B. Wolff, T. A. Mancini, P. Pouliquen, and A. G. Andreou, "Liquid crystal polarization camera," IEEE Trans. on Robotics and Automation **13**, 195–203 (1997).

8. L. B. Wolff, and A. G. Andreou, "Polarization camera sensors," Image and Vision Computing Journal **13**, 497–510 (1995).

9. W. G. Egan, W. R. Johnson, and V. S. Whitehead, "Terrestrial polarization imagery obtained from the Space Shuttle: characterization and interpretation," Applied Optics **30**, 435–442 (1991).

10. F. Goudail, P. Terrier, Y. Takakura, L. Bigue, F. Galland, and V. DeVlaminck, "Target detection with a liquid-crystal-based passive Stokes polarimeter," Applied Optics **43**, 274–282 (2004).

11. F. Goudail and P. Réfrégier, "Statistical algorithms for target detection in coherent active polarimetric images," J. Opt. Soc. Am. A **18**, 3049–3060 (2001).

12. F. Goudail and P. Réfrégier, "Statistical techniques for target detection in polarization diversity images," Opt. Lett. **26**, 644-646 (2001).

13. J. S. Tyo, M. P. Rowe, E. N. Pugh, Jr., and N. Engheta, "Target detection in optically scattered media by polarization-difference imaging", Applied Optics **35**, 1855–1870 (1996).

14. Y. Y. Schechner, S. G. Narasimhan, and S. K. Nayar, "Polarization-based vision through haze," Applied Optics **42**, 511-525 (2003).

15. Y. Y. Schechner and N. Karpel, "Clear underwater vision," *Proc. of IEEE Computer Society Conference on Computer Vision and Pattern Recognition* (Institute of Electrical and Electronics Engineers, 2004), 536-543.

16. Y. Y. Schechner and N. Karpel, "Recovery of underwater visibility and structure by

polarization analysis," IEEE Journal of Oceanic Engineering **30**, 570–587 (2005).

17. Y. Y. Schechner, J. Shamir, and N. Kiryati, "Vision through semireflecting media: polarization analysis," Opt. Lett. **24**, 1088-1090 (1999).

18. P. C. Y. Chang, J. C. Flitton, K. I. Hopcraft, E. Jakeman, D. L. Jordan, and J. G. Walker, "Improving visibility depth in passive underwater imaging by use of polarization," Appl. Opt. 42, 2794-2803 (2003).

19. J. G. Walker, P. C. Y. Chang, and K. I. Hopcraft, "Visibility depth improvement in active polarization imaging in scattering media," Appl. Opt. **39**, 4933–4941 (2000).

20. H. Wang, C. Sun, Y. Wang, Y. Kiang, and C. Yang, "Determination of the depth of a scattering target in a turbid medium with polarization discrimination of transmitted signals," Opt. Lett. **28**, 25-27 (2003).

21. S. G. Demos, W. B. Wang, and R. R. Alfano, "Imaging objects hidden in scattering media with fluorescence polarization preservation of contrast agents," Appl. Opt. **37**, 792–797 (1998).

22. A. M. Wallace, B. Liang, E. Trucco, and J. Clark, "Improving depth acquisition using polarized light," Int. Journal of Computer Vision **32**, 87–109 (2001).

23. R. Nothdurft and G. Yao, "Expression of target optical properties in subsurface polarization-gated imaging," Opt. Express **13**, 4185-4195 (2005).

24. H. Chen and L. B. Wolff, "Polarization phase-based method for material classification and object recognition in computer vision," *Proc. of IEEE Computer Society Conference on Computer Vision and Pattern Recognition* (Institute of Electrical and Electronics Engineers, 1996), 128–135.

25. L. B. Wolff, "Polarization-based material classification from specular reflection," IEEE Trans. on Pattern Analysis and Machine Intelligence **12**, 1059–1071 (1990).

26. Although, human visual system does not have an ability to sense polarized light, the polarization is still might be perceptible in the form of Haidinger's brush.

27. K. von Frisch, "Die polarisation des himmelslichtes als orientierender faktor bei den tanzen der bienen", Experientia **5**, 142–148 (1949).

28. K. von Frisch, *Tanzsprache und Orientierung der Bienen* (Berlin, Springer, 1965).

29. K. von Frisch, "Nobel Lecture," http://www.nobel.se/medicine/laureates/1973/frisch-lecture.pdf.

30. R. Wehner and G. D. Bernard, "Photoreceptor twist: a solution to the false colour problem," Proc. Natl. Acad. Sci. USA **90**, 4132-4135 (1993).

31. R. Wehner, "Polarized-light navigation by insects," Scientific American **235**, 106–114 (1976).

32. R. Wehner, "Neurobiology of polarization vision," Trends in Neurosciences **12**, 353-359 (1989).

33. R. Wehner, "'Matched filters' – neural models of the external world," Journal of Comparative Physiology A **161**, 511-531 (1987).

34. I. Pomozi, G. Horváth, and R. Wehner, "How the clear-sky angle of polarization pattern continues underneath clouds: full-sky measurements and implications for animal orientation," The Journal of Experimental Biology **204**, 2933–2942 (2001).

35. G. Horváth, J. Gál, T. Labhart, and R Wehner, "Does reflection polarization by plants influence colour perception in insects? Polarimetric measurements applied to a polarization-sensitive model retina of Papilio butterflies," The Journal of Experimental Biology **205**, 3281–3298 (2002).

36. T. Labhart, "Polarization opponent interneurones in the insect visual system," Nature **331**, 435–437 (1988).

37. C. W. Hawryshyn, "Polarization Vision in Fish," American Scientist, **80,** 164–175, 1992.

38. C. W. Hawryshyn, "Ultraviolet polarization vision in fishes: Possible mechanisms for coding e-vector," Phil. Trans. R. Soc. London, Ser B **355**, 1187–1190 (2000).

39. N. Shashar, and T. W. Cronin, "Polarization contrast vision in octopus," The Journal of Experimental Biology **199**, 999-1004 (1996).

40. T. W. Cronin, N. Shashar, "The linearly polarized light field in clear, tropical marine waters: spatial and temporal variation of light intensity, degree of polarization and e-vector angle," The Journal of Experimental Biology **204**, 2461–2467 (2001).

41. N. Shashar, P. S. Rutledge, and T. W. Cronin, "Polarization vision in cuttlefish - A concealed communication channel?" The Journal of Experimental Biology **199**, 2077-2084 (1996).

42. T. W. Cronin, N. Shashar, R. L. Caldwell, J. Marshall, A. G. Cheroske, and T.-H. Chiou, "Polarization Vision and Its Role in Biological Signaling," Integrative and Comparative Biology **43**, 549–558 (2003).

43. M. P. Rowe, E. N. Pugh, Jr., J. S. Tyo, and N. Engheta, "Polarization-difference imaging: a biologically inspired technique for observation through scattering media", Opt. Lett. **20**, 608–610 (1995).

44. J. S. Tyo, E. N. Pugh, Jr., and N. Engheta, "Colorimetric representation for use with polarization-difference imaging of objects in scattering media", J. Opt. Soc. Am. A **15**, 367–374 (1998).

45. K. M. Yemelyanov, M. A. Lo, E. N. Pugh, Jr., and N. Engheta, "Display of polarization information by coherently moving dots," Optics Express **11**, 1577-1584 (2003), http://www.opticsexpress.org/abstract.cfm?URI=OPEX-11-13-1577.

46. K. M. Yemelyanov, S.-S. Lin, W. Q. Luis, E. N. Pugh, Jr., and N. Engheta, "Bio-inspired display of polarization information using certain visual cues," *in Proceedings of SPIE* (SPIE-The International Society for Optical Engineering, San Diego, CA, 2003), 71-84.

47. T. Labhart, "How polarization-sensitive interneurons perform at low degrees of polarization," J. Experimental Biology 199, 1467–1475 (1996).

48. T. Labhart and E. P. Meyer, Neural mechanisms in insect navigation: polarization compass and odometer, Current Opinion in Neurobiology **12**,707–714 (2002).

49. W. B. Wang, S. G. Demos, J. Ali, and R. R. Alfano, "Imaging fluorescent objects embedded inside animal tissues using polarization-difference technique," Optics Communication **142**, 161–166 (1997).

50. C. K. Harnett and H. G. Craighead, "Liquid-crystal micropolarizer array for polarization-difference imaging," Applied Optics **41**, 1291–1296 (2002).

51. S. P. Schilders, X. S. Gan, and M. Gu, "Resolution improvement in microscopic imaging through turbid media based on differential polarization gating," Applied Optics, **37**, 4300-4303 (1998).

52. M. Born and E. Wolf, Principles of Optics, 7th ed. (Cambridge University Press, New York, 2002).

53. As "regular" or "conventional" PDI in this paper we always refer to the technique introduced in [43].

54. G. Buchsbaum and A. Gottschalk, "Trichromacy, opponent colours coding and optimum colour information transmission in the retina," Proc. R. Soc. London, Ser. B **220**, 89–113 (1983).

55. N. A. Macmillan and C. D. Creelman, *Detection Theory: A User's guide* (Cambridge University Press, London, 1991).

56. I. T. Jolliffe, *Principal Component Analysis* (Springer-Verlag, New-York, 1986).

57. S.-S. Lin, K. M. Yemelyanov, E. N. Pugh, Jr., and N. Engheta, "Polarization Enhanced Visual Surveillance Techniques," *in Proc. IEEE International Conference on Networking, Sensing, and Control* (Institute of Electrical and Electronics Engineers, Taipei, Taiwan, 2004), pp. 216-221.

10. List of Figure Captions

Figure 1. Layout of the experimental setup: *a*) Photograph of the setup, *b*) 7-patch target together with a US 10 cent, "dime", coin.

Figure 2. Normalized histograms of polarization parameters of the background: A) Half of total pixel intensity, I_U; B) Degree of linear polarization, p; C) Angle of polarization, θ. Total number of pixels in the image was 800x600. Images of I_U and p in the top row are stretched to cover 8-bit grayscale range. The reason we have systematic variations in the images of I_U and p is that the light comes from the one side (top left corner in the Figure).

Figure 3. Normalized histogram of the "dark noise" of the camera (a) compared to the normalized histogram of the background image (b).

Figure 4. Distribution of the polarization parameters characterizing the standard "background" scene. Each panel presents a pseudo-color representation of the distribution of one of the parameters: A) $\alpha(\varphi_1,\varphi_2)$, B) $\beta(\varphi_1,\varphi_2)$, C) $\lambda_1(\varphi_1,\varphi_2)$, D) $\lambda_2(\varphi_1,\varphi_2)$. The scales for each parameter are provided to the right of each panel.

Figure 5. Principal components of the scene corresponding to three cases of interest. Left column shows PC_1, and right column PC_2 images, respectively. Panels *a*), *b*) and *c*) correspond to cases # 1, 2, and 3, respectively. All images are linearly rescaled to exploit 8-bit displayable range. The size of the images was 800 by 600 pixels.

Figure 6. Normalized histograms of PC_1 (a), PC_2 (b) for all the cases shown as images in Figure 5. The standard deviations of PCs for all three cases considered are shown in the figures.

Figure 7. The scheme of the specially created target with regions used for the sensitivity index calculation marked in blue color. Red lines identify the direction of scratches in the specific patch. The left side region is referred to as "region one", and the right side region is referred to as "region two", respectively.

Figure 8. Polarization components for the "non-target" and "target" scenes of the experiments under natural lighting. The left panel shows I_U, p, and θ (top to bottom) image of the "non-target" scene, and the right panel shows those for the "target" scene. The I_U plots in both cases are linearly rescaled to use the full 8-bit grayscale display range.

Figure 9. Comparison in target detection between images obtained by our new adaptive algorithm and by the conventional PDI algorithm. They are the principal components images obtained from the images shown in Figure 8. Panels a), b) are PC_1 and PC_2 for Case #1. Panels c) and d) are conventional PS and PD images (Case #3). Panels e) and f) are PC_1 and PC_2 for the Case #2. All images were linearly rescaled to cover 8-bit gray level display range.

Figure 10. A) Signal to noise ratio for the PC_1 and PC_2. Here the signal is the area of the aluminum disk and the noise is the rest area of the corresponding PC. B) Normalized histograms of the PC_2 images with shifted from the "optimal" (Case #1) pair of angles. Increasing variance in the PC_2 image with rotation of the optimal pair of angles is shown.

Figure 11. Signal to noise ratios for the PC_1, PC_2, *PS*, *PD*, and p with the presence of artificially added Gaussian noise A), and white noise B). Images of PC_2 C) and p D) for 5% of added Gaussian noise. Individual features of the aluminum disk, such as appearance of patches, is better visible in PC_2 image.

Figure 12. A), B) Stretched images of PC_2 and p, respectively, C) Normalized histograms of images shown in panels A), B). Standard deviations for PC_2 and p are $\sigma^2 = 0.0054$ and $\sigma^2 = 0.041$, respectively.

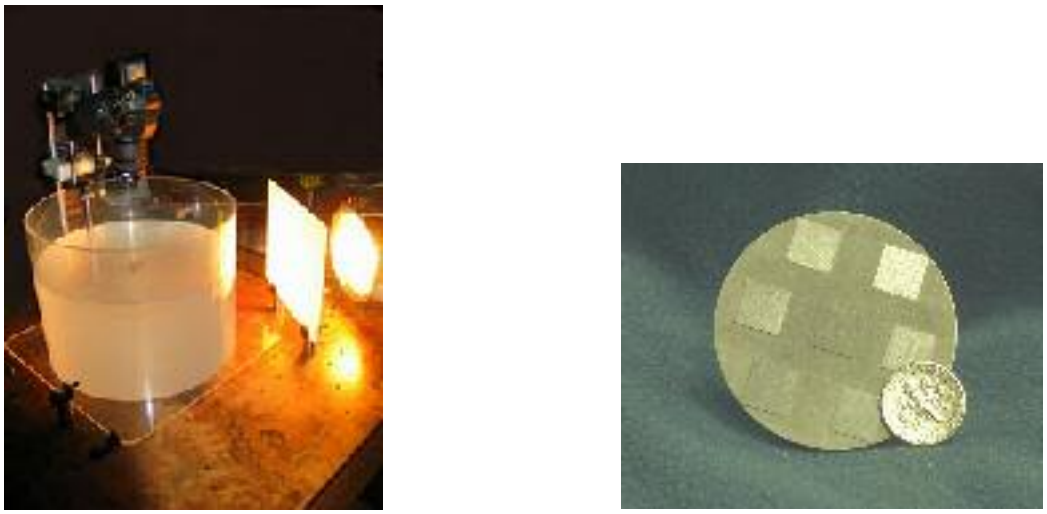

(a) (b)

Figure 1. Layout of the experimental setup: *a*) Photograph of the setup, *b*) 7-patch target together with a US 10 cent, "dime", coin.

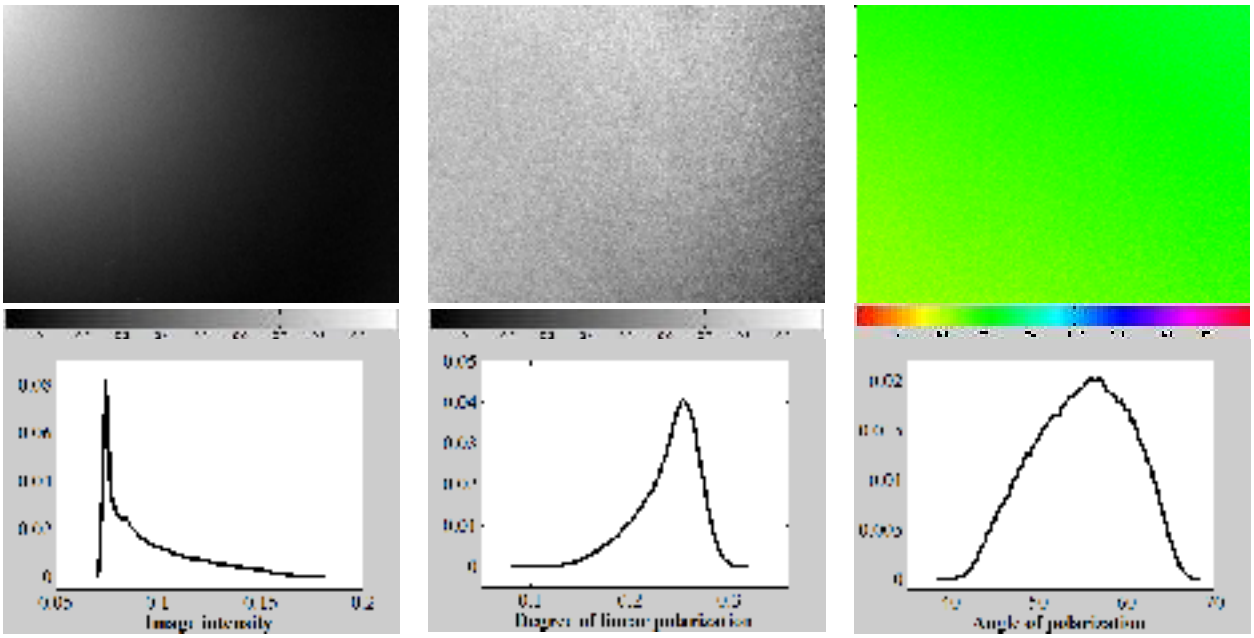

a) *b*) *c*)

Figure 2. Normalized histograms of polarization parameters of the background: A) Half of total pixel intensity, I_U ; B) Degree of linear polarization, p ; C) Angle of polarization, θ . Total number of pixels in the image was 800x600. Images of I_U and p in the top row are stretched to cover 8-bit grayscale range. The reason we have systematic variations in the images of I_U and p is that the light comes from the one side (top left corner in the Figure).

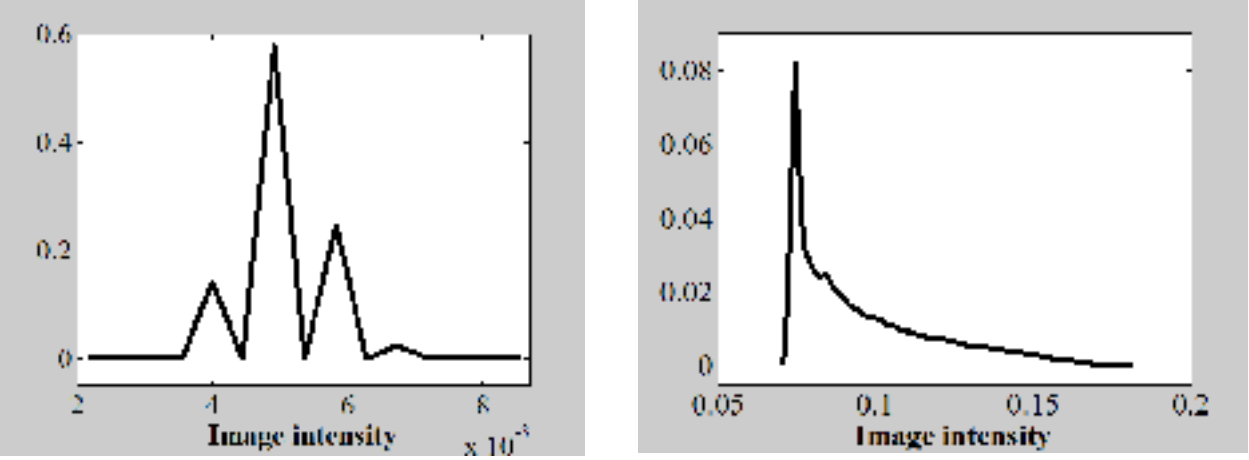

a) *b)*

Figure 3. Normalized histogram of the "dark noise" of the camera (a) compared to the normalized histogram of the background image (b).

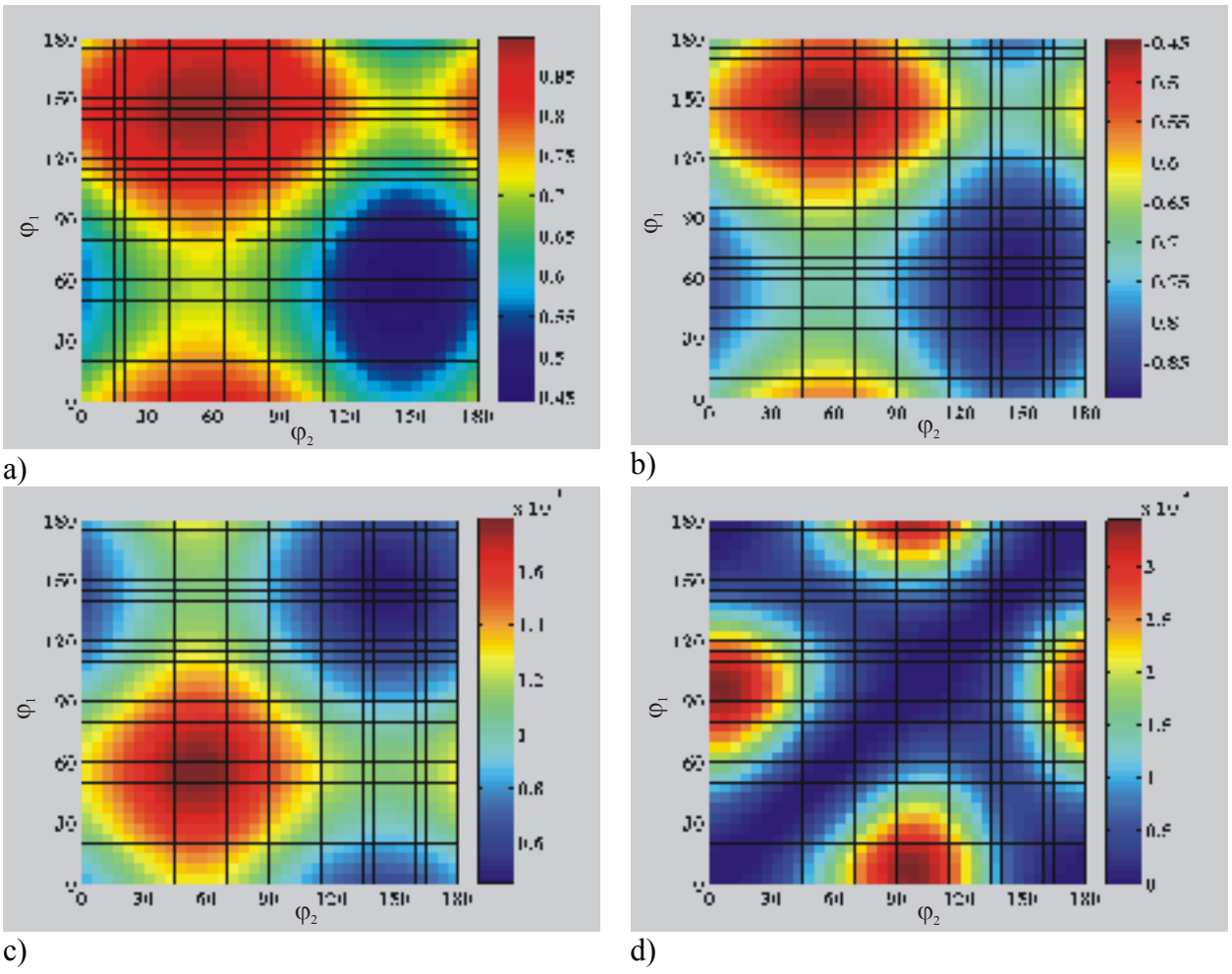

Figure 4. Distribution of the polarization parameters characterizing the standard "background" scene. Each panel presents a pseudo-color representation of the distribution of one of the parameters: A) $\alpha(\varphi_1,\varphi_2)$, B) $\beta(\varphi_1,\varphi_2)$, C) $\lambda_1(\varphi_1,\varphi_2)$, D) $\lambda_2(\varphi_1,\varphi_2)$. The scales for each parameter are provided to the right of each panel.

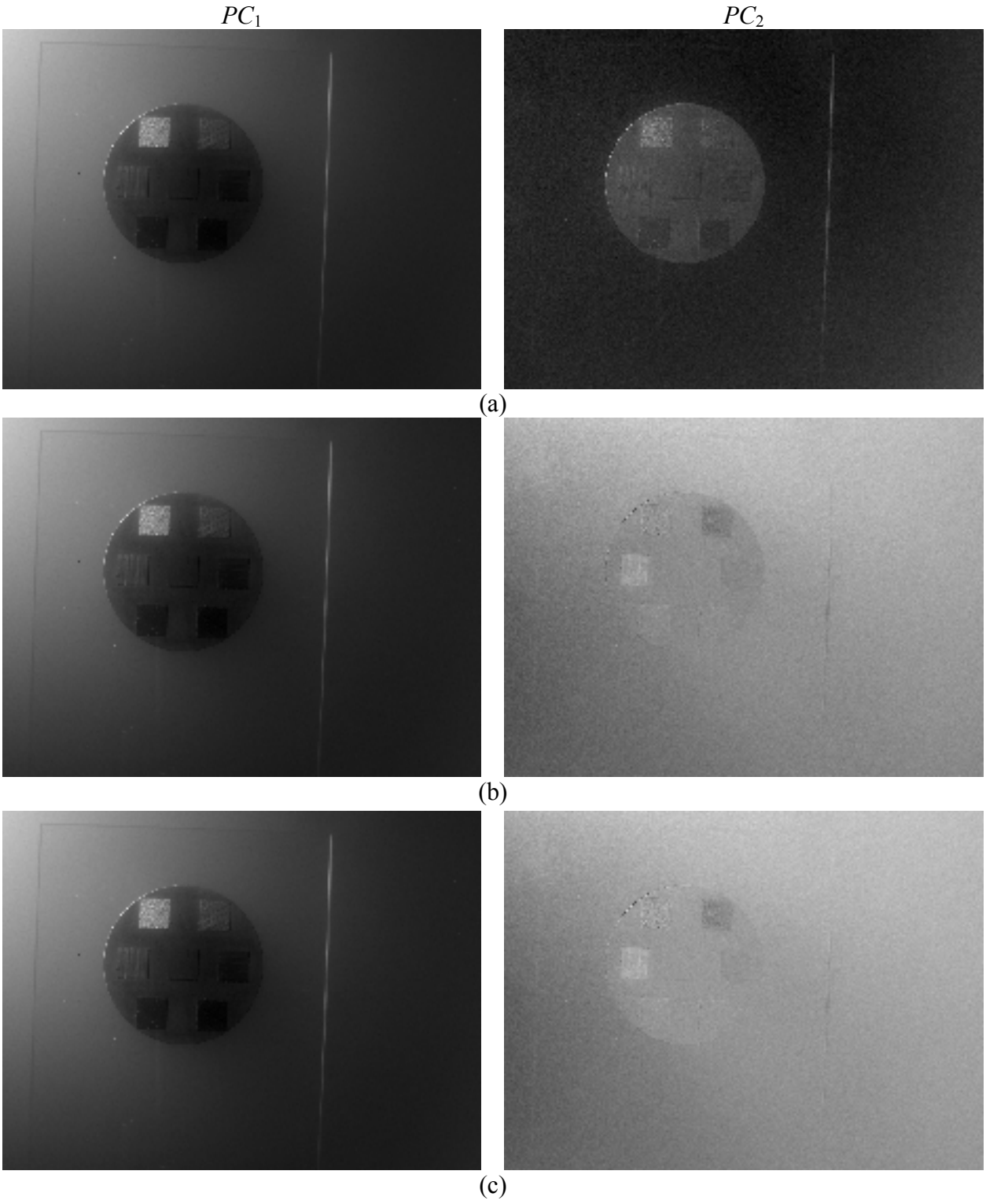

Figure 5. Principal components of the scene corresponding to three cases of interest. Left column shows PC_1, and right column PC_2 images, respectively. Panels *a*), *b*) and *c*) correspond to cases # 1, 2, and 3, respectively. All images are linearly rescaled to exploit 8-bit displayable range. The size of the images was 800 by 600 pixels.

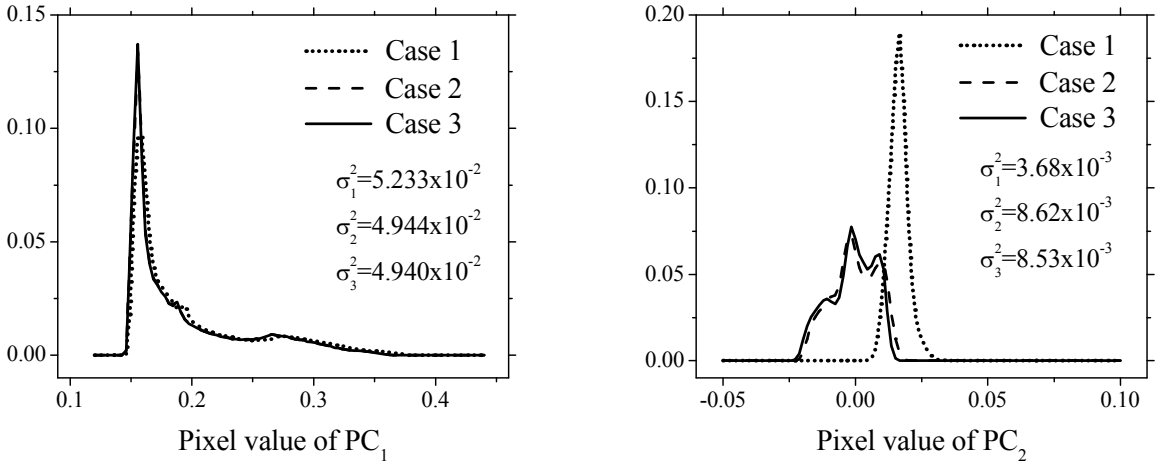

a) b)

Figure 6. Normalized histograms of PC_1 (a), PC_2 (b) for all the cases shown as images in Figure 5. The standard deviations of PCs for all three cases considered are shown in the figures.

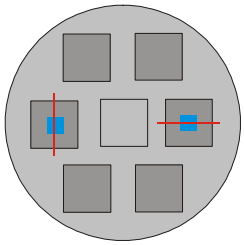

Figure 7. The scheme of the specially created target with regions used for the sensitivity index calculation marked in blue color. Red lines identify the direction of scratches in the specific patch. The left side region is referred to as "region one", and the right side region is referred to as "region two", respectively.

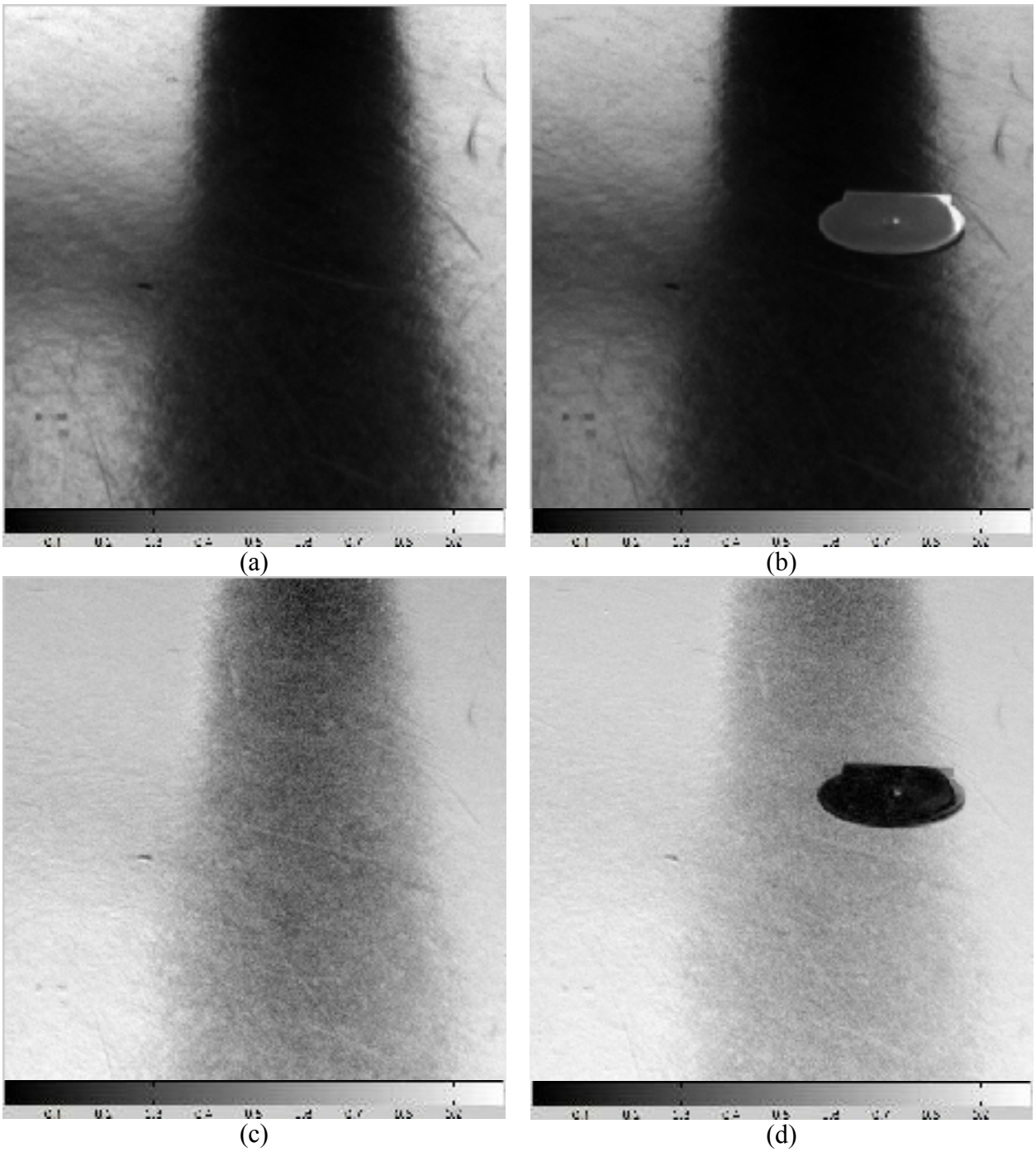

(a) (b)

(c) (d)

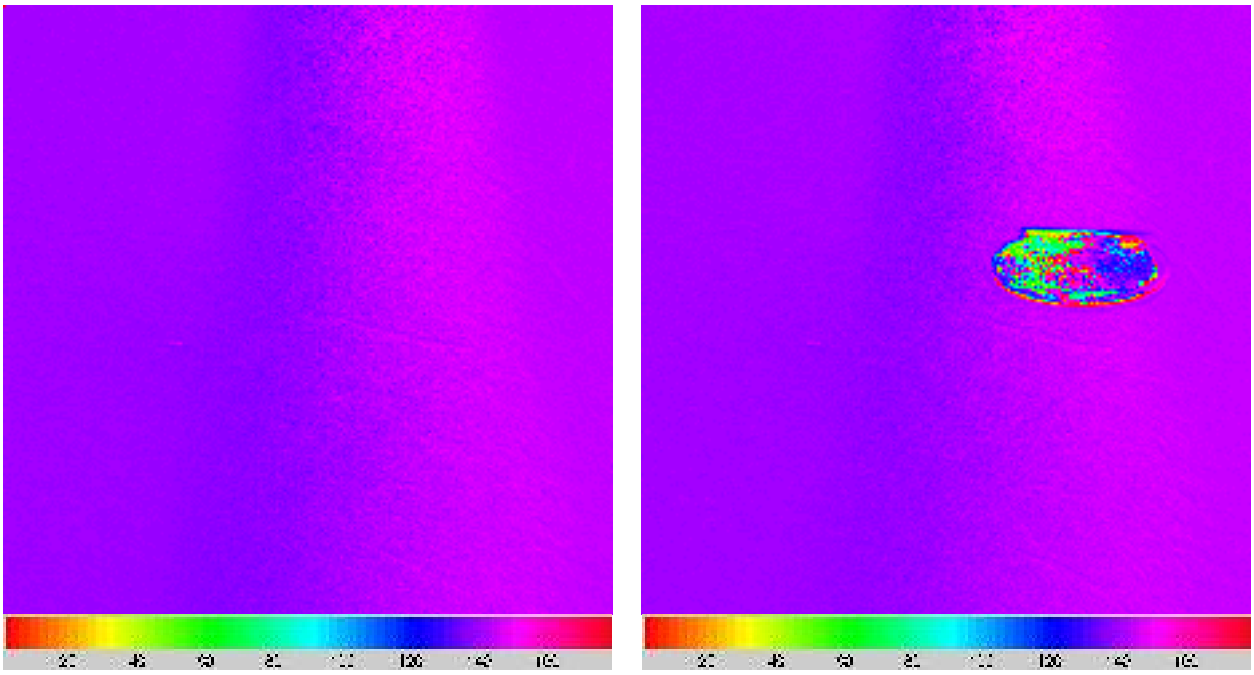

(e) (f)

Figure 8. Polarization components for the "non-target" and "target" scenes of the experiments under natural lighting. The left panel shows I_U, p, and θ (top to bottom) image of the "non-target" scene, and the right panel shows those for the "target" scene. The I_U plots in both cases are linearly rescaled to use the full 8-bit grayscale display range.

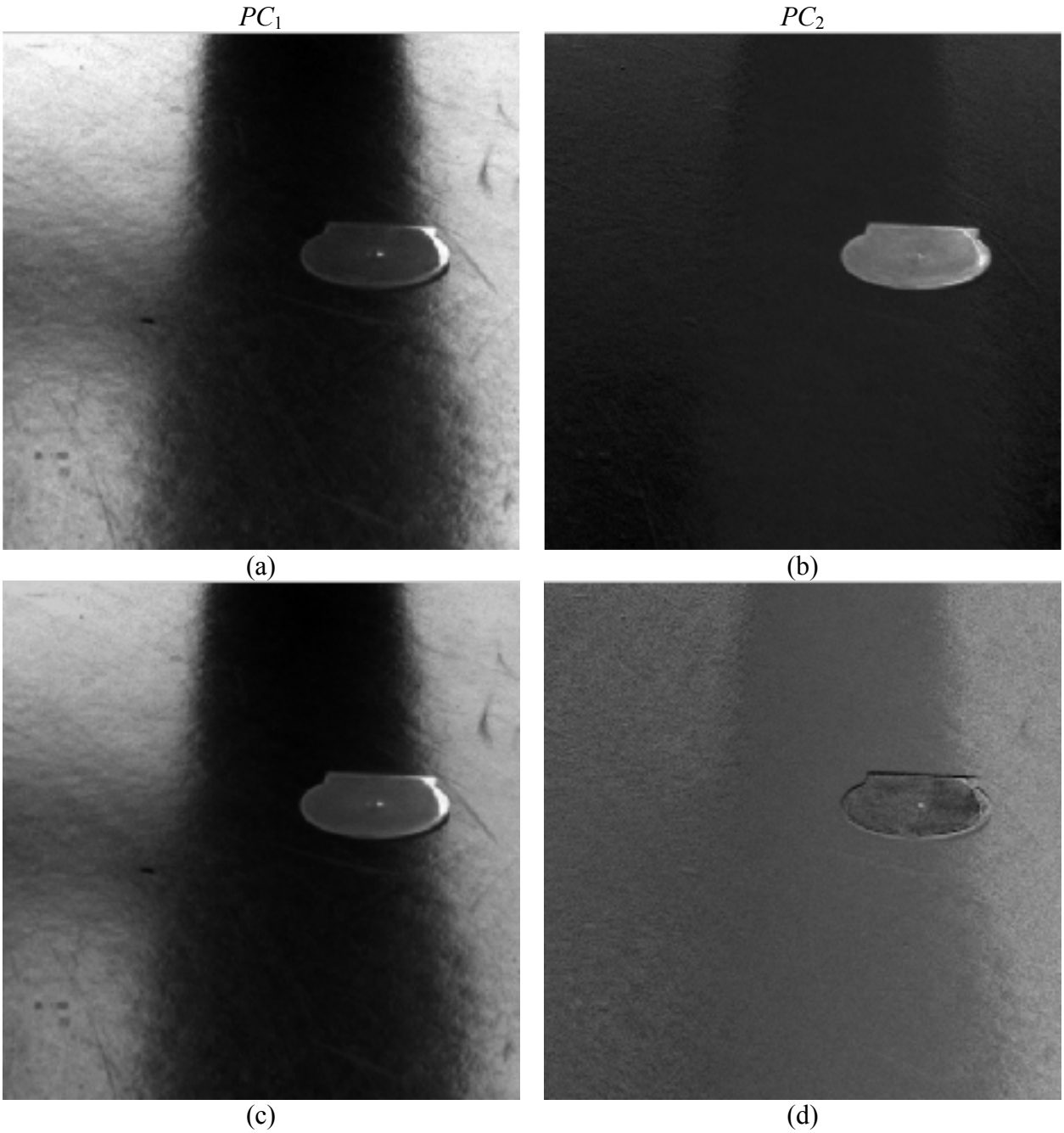
PC_1
PC_2
(a)
(b)
(c)
(d)

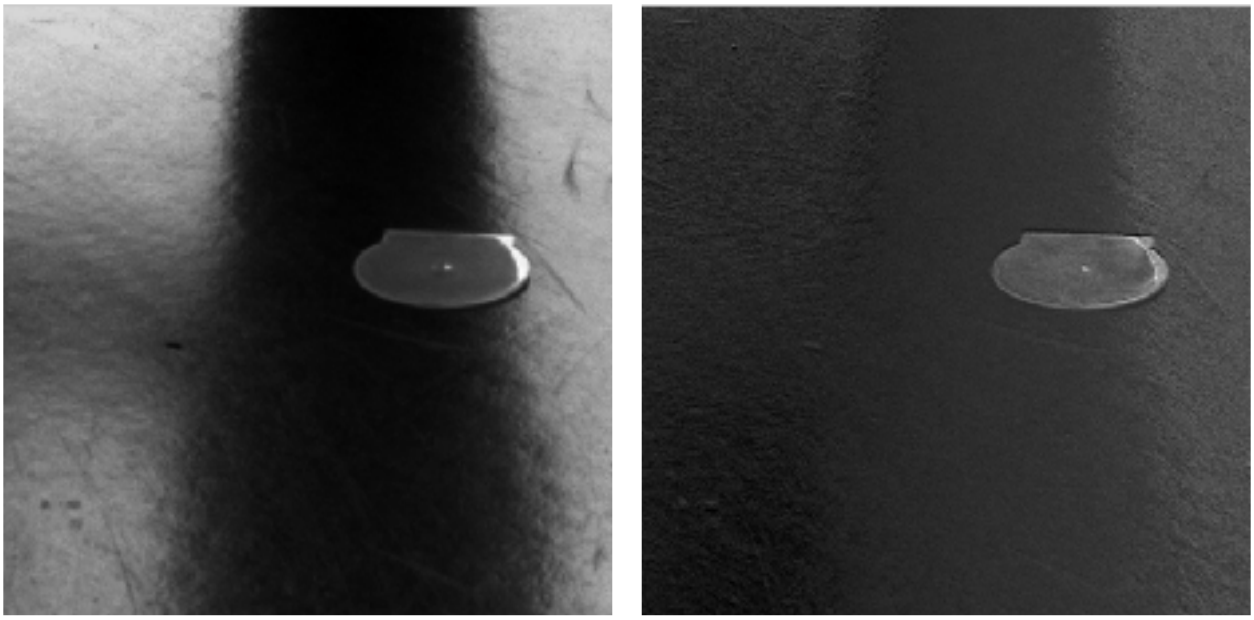

(e) (f)

Figure 9. Comparison in target detection between images obtained by our new adaptive algorithm and by the conventional PDI algorithm. They are the principal components images obtained from the images shown in Figure 8. Panels a), b) are PC_1 and PC_2 for Case #1. Panels c) and d) are conventional PS and PD images (Case #3). Panels e) and f) are PC_1 and PC_2 for the Case #2. All images were linearly rescaled to cover 8-bit gray level display range.

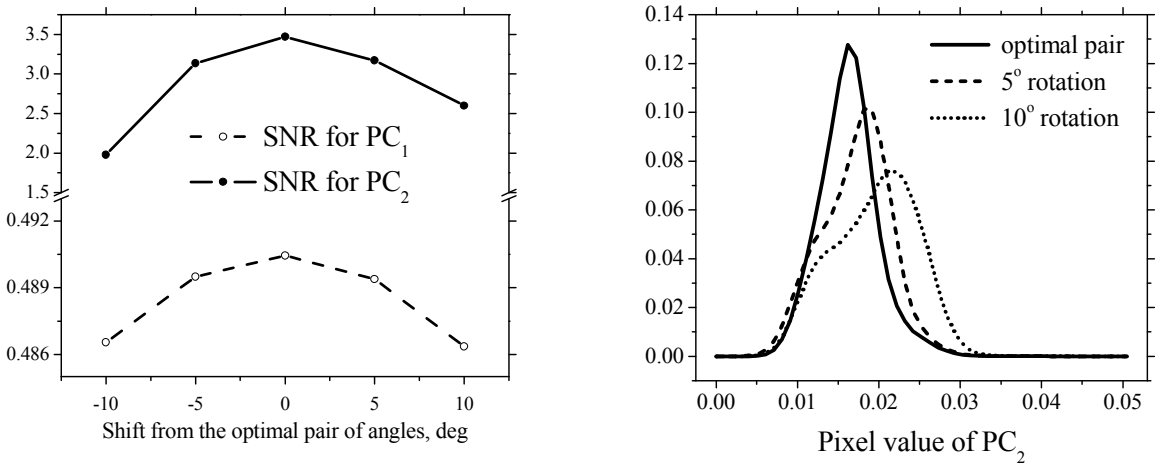

a) b)

Figure 10. A) Signal to noise ratio for the PC_1 and PC_2. Here the signal is the area of the aluminum disk and the noise is the rest area of the corresponding PC. B) Normalized histograms of the PC_2 images with shifted from the "optimal" (Case #1) pair of angles. Increasing variance in the PC_2 image with rotation of the optimal pair of angles is shown.

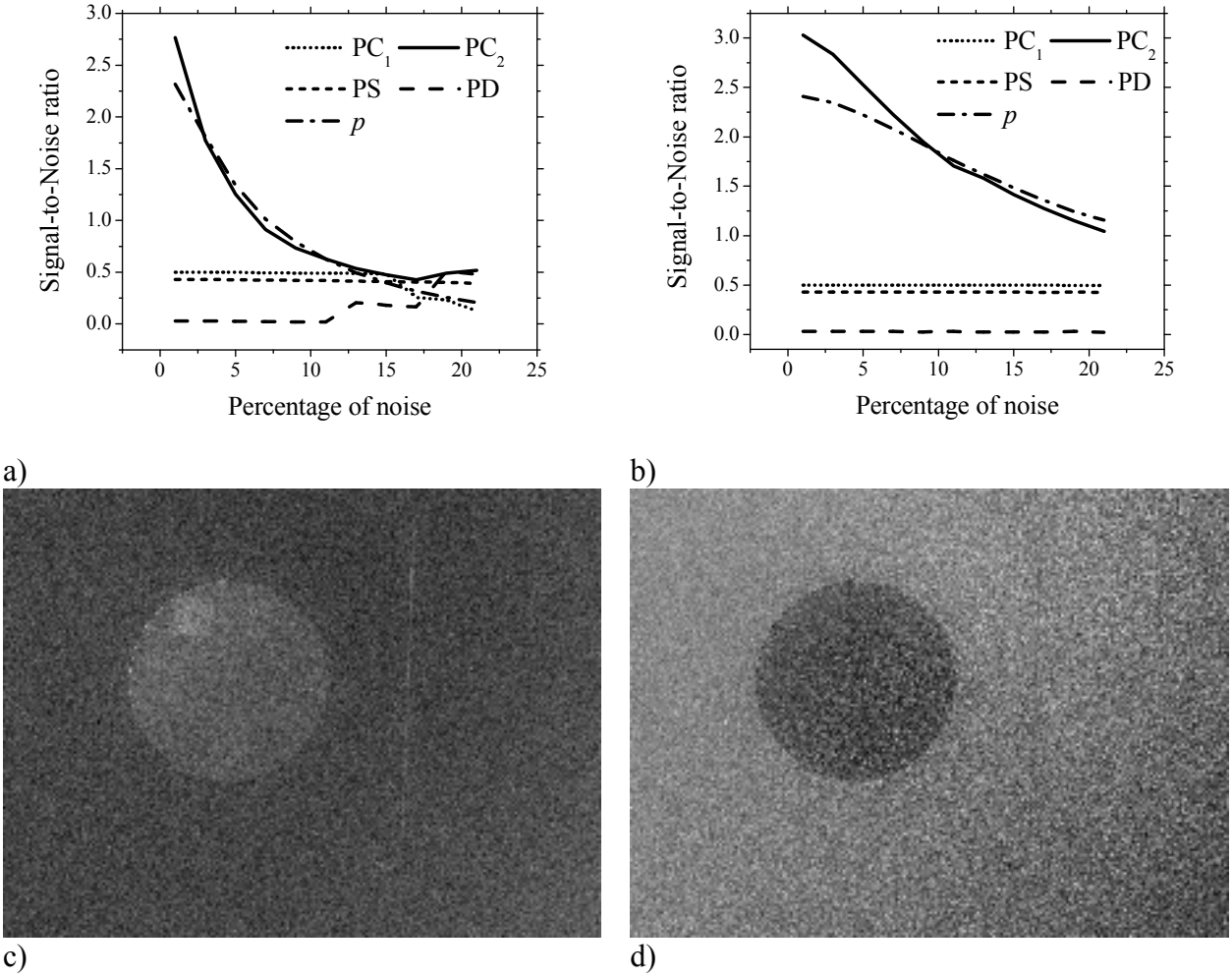

Figure 11. Signal to noise ratios for the PC_1, PC_2, *PS*, *PD*, and p with the presence of artificially added Gaussian noise A), and white noise B). Images of PC_2 C) and p D) for 5% of added Gaussian noise. Individual features of the aluminum disk, such as appearance of patches, is better visible in PC_2 image.

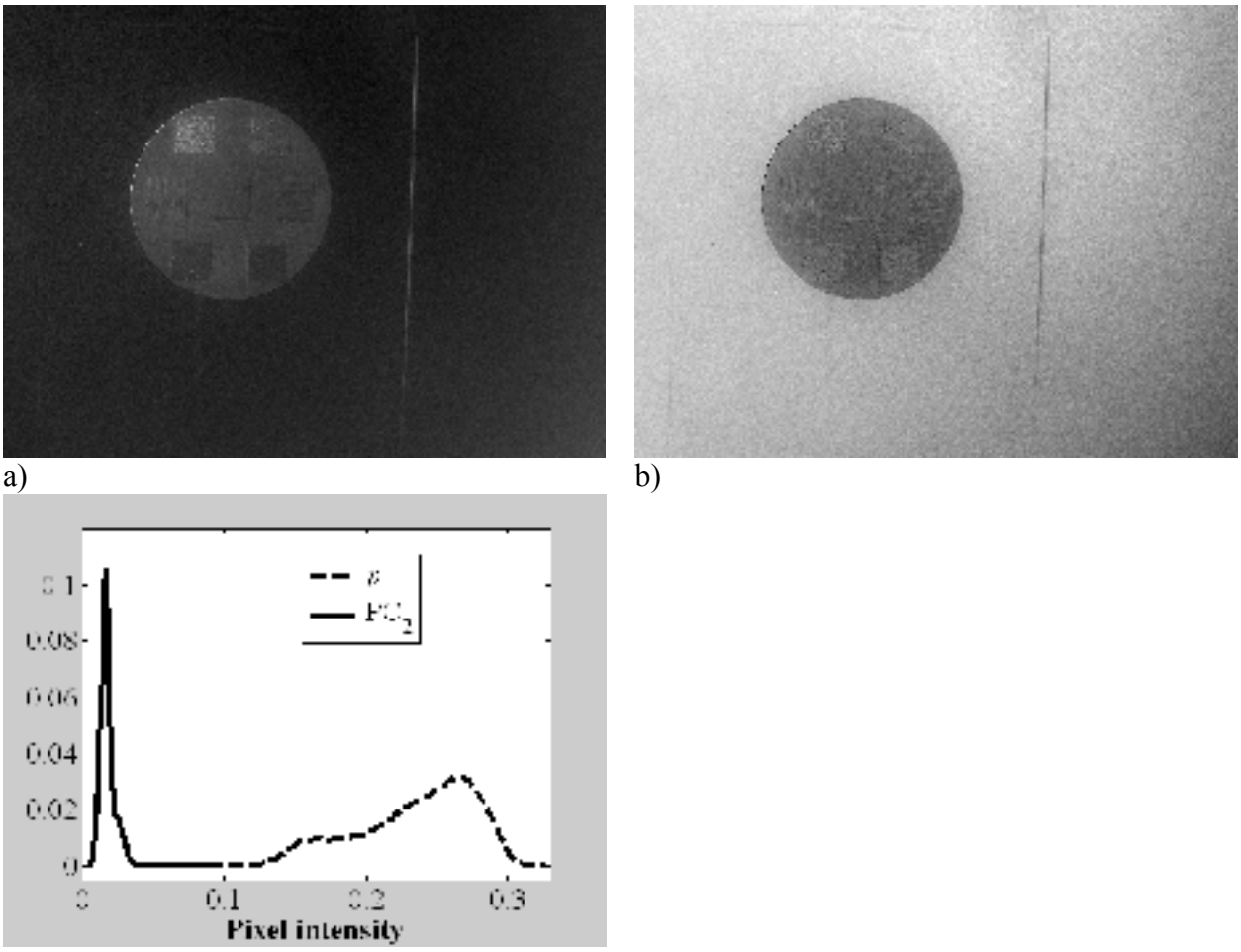

Figure 12. A), B) Stretched images of PC_2 and p, respectively, C) Normalized histograms of images shown in panels A), B). Standard deviations for PC_2 and p are $\sigma^2 = 0.0054$ and $\sigma^2 = 0.041$, respectively.

Table 1 Adaptive parameters corresponding to the cases considered for the benchmark target

	φ_1, deg	φ_2, deg	α	β	$\lambda_1 \times 10^{-3}$	$\lambda_2 \times 10^{-5}$
Case #1	145	55	0.895	–0.446	1.116	0.611
Case #2	95	5	0.680	–0.733	1.005	3.447
Case #3	100	10	0.707	–0.707	1.004	3.327